Gradients estimation from random points with volumetric tensor in turbulence

Tomoaki Watanabe[a,1,*], Koji Nagata[a]

[a]*Department of Aerospace Engineering, Nagoya University, Nagoya 464-8603, Japan*

Abstract

We present an estimation method of fully-resolved/coarse-grained gradients from randomly distributed points in turbulence. The method is based on a linear approximation of spatial gradients expressed with the volumetric tensor, which is a 3×3 matrix determined by a geometric distribution of the points. The coarse grained gradient can be considered as a low pass filtered gradient, whose cutoff is estimated with the eigenvalues of the volumetric tensor. The present method, the volumetric tensor approximation, is tested for velocity and passive scalar gradients in incompressible planar jet and mixing layer. Comparison with a finite difference approximation on a Cartesian grid shows that the volumetric tensor approximation computes the coarse grained gradients fairly well at a moderate computational cost under various conditions of spatial distributions of points. We also show that imposing the solenoidal condition improves the accuracy of the present method for solenoidal vectors, such as a velocity vector in incompressible flows, especially when the number of the points is not large. The volumetric tensor approximation with 4 points poorly estimates the gradient because of

*Corresponding author (+81-052-789-3279)
Email address: watanabe.tomoaki@c.nagoya-u.jp (Tomoaki Watanabe)

anisotropic distribution of the points. Increasing the number of points from 4 significantly improves the accuracy. Although the coarse grained gradient changes with the cutoff length, the volumetric tensor approximation yields the coarse grained gradient whose magnitude is close to the one obtained by the finite difference. We also show that the velocity gradient estimated with the present method well captures the turbulence characteristics such as local flow topology, amplification of enstrophy and strain, and energy transfer across scales.
Keywords: Volumetric tensor, Spatial derivative, Turbulence, Lagrangian simulations

1. Introduction

Spatial gradients of physical quantities play important roles in many physics problems. In fluid dynamics, the velocity gradient tensor is of great importance in modeling and data analysis of turbulent flows.[1,2] The gradient of scalar quantities, such as mass fractions of chemicals and temperature, are as important as the velocity gradient in combustion modeling.[3] Velocity or other quantities in numerical simulations are obtained at discrete points in space. The spatial gradients are easily computed with finite differences when the spatial discretization is based on a structured grid. The situations become much more complicated when the data is stored at randomly distributed points. We encounter this problem in Lagrangian simulations, where the variables are stored along with fluid particle trajectories. Examples can be found in numerical simulations of turbulent reacting flows based on Lagrangian particles,[4,5,6] where a scalar field is represented by Lagrangian

fluid particles to which scalar values are assigned.[7] The particles are tracked with a velocity field computed in an Eulerian simulation using a grid. These simulations require the estimation of scalar gradients or relevant quantities (e.g. scalar dissipation rate and mixing timescale) on randomly distributed particle positions. This has been done in most simulations with interpolation of the values computed on a grid onto the particle positions, which requires an additional Eulerian simulations of a so-called reference scalar or procedures for dynamically determining model parameters.[5,8,9] The models implemented in these simulations often use the coarse grained gradient, which does not contain the contribution from small scale structures. The coarse grained gradient can be interpreted as a low pass filtered field, and being combined with subgrid scale models, it is used for computing the quantities related to a gradient of a fully resolved field.[10]

Development of the estimation method of fully-resolved/coarse-grained gradients from randomly distributed points is expected to contribute the progress of Lagrangian simulations of fluid dynamics problems. One of the important attempts for coarse grained gradients was done by Chertkov et al.,[11] where tetrads consisting of four Lagrangian particles are used for estimating the velocity gradient tensor at large scales. A similar approach has been also used in computation of gradient in simulations with non-curvilinear spherical grids.[12,13,14] In this study, we consider the gradient estimation from multiple points using a volumetric tensor, which characterizes the spatial distribution of points. The present approach with the volumetric tensor has been used in the analysis of data recorded by multiple spacecrafts.[15] However, no attempt has been reported to examine the performance of the gradient

estimation with the volumetric tensor in turbulent flows in comparison with other methods (e.g. finite difference). It is not clear whether this method is capable of estimating the coarse grained gradient in turbulence, where gradient fields strongly depend on the scale. We test the gradient estimation method with the volumetric tensor for a wide range of scales using the DNS database of turbulent flows. In fluid dynamics problems, introducing the volumetric tensor is shown to be important for the following reasons: the volumetric tensor makes the gradient estimation method general and applicable under various conditions without changing the procedure; the volumetric tensor determines the length scale of the coarse grained gradient from the particle distribution. The latter is crucial in the application of the present gradient estimation method to numerical simulations because the cutoff length scale of coarse grained gradients often appears in subgrid scale models used in large eddy simulations.[10]

We describe the gradient estimation method based on the volumetric tensor, which is defined for randomly distributed points in Sec. 2, where the gradients are considered for scalar, vector, and solenoidal vector. The present methods are tested with the DNS database of turbulent planar jet and mixing layer. The detail of the DNS and the procedure for testing the present method are described in Sec. 3. Section 4 discusses the performance of the gradient estimation method in comparison with a conventional finite difference approximation. Finally, conclusion is summarized in Sec. 5.

2. Spatial gradient estimation with volumetric tensor

2.1. Volumetric tensor for spatially distributed points

We present the method to estimate spatial gradients of scalar or vector quantities from the values given at non-uniformly distributed points. We consider N points ($N \geq 4$), where nth point is located at $\mathbf{x}^{(n)}$ ($n = 1, ..., N$). The center position of the N points is given by $\mathbf{x}_0 = \overline{\mathbf{x}} = (1/N)\sum_{n=1}^{N} \mathbf{x}^{(n)}$, where the overbar denotes the average of N points. The location of each point relative to the center is $\mathbf{r}^{(n)} = \mathbf{x}^{(n)} - \mathbf{x}_0$. The geometric distribution of the points is described by the volumetric tensor R_{ij} defined as[16]

$$R_{ij} = \overline{r_i r_j} = \frac{1}{N}\sum_{n=1}^{N} r_i^{(n)} r_j^{(n)}. \tag{1}$$

The volumetric tensor plays an important role in the gradient estimation discussed below. This tensor was also used for studying the deformation of fluid volume in turbulent flows.[17] R_{ij} has three real eigenvalues denoted by R_a^2, R_b^2, and R_c^2 and ranging from largest to smallest ($R_a^2 \geq R_b^2 \geq R_c^2$) with the corresponding eigenvectors $\boldsymbol{a}$, $\boldsymbol{b}$, and $\boldsymbol{c}$. When we use a quasi-ellipsoid shape as an approximation of the distribution of the points, this shape is well represented by the eigenvalues of the volumetric tensor,[15] where the major, middle, and minor semi axes are, respectively, given by R_a, R_b, and R_c while their directions are $\boldsymbol{a}$, $\boldsymbol{b}$, and $\boldsymbol{c}$. Then, the eigenvalues of the volumetric tensor can be related to the volume of the quasi-ellipsoid for N points as $V = (4\pi/3)R_a R_b R_c$. The shape of the quasi-ellipsoid can be characterized by two parameters called elongation and planarity, which are defined as $E = 1 - R_2/R_1$ and $P = 1 - R_3/R_2$, respectively.[15] When the points lie nearly on a straight line, $E \approx 1$ because of $R_2 \approx R_3 \approx 0$. When

the points lie nearly on a plane, $R_2 \gg R_3 \approx 0$ resulting in $P \approx 1$. Both E and P have a small value when the distribution of the points is isotropic and characterized by a pseudo-sphere.

2.2. Spatial gradient of scalar quantities

We can use the cluster of points to estimate a coarse grained gradient in turbulent flows following the analysis method for multi-spacecraft data.[16] The estimated spatial gradient depends on the shape and size of the cluster, which are characterized by the volumetric tensor as discussed above. Here, we consider the gradient of a scalar quantity ϕ, which is represented by $\phi_{,i} \equiv \partial\phi/\partial x_i$. Hereafter, we denote ϕ and $\partial\phi/\partial x_i$ evaluated at a point $\mathbf{x}^{(n)}$ as $\phi^{(n)}$ and $\phi^{(n)}_{,i}$, respectively. We can express an ensemble average of ϕ for all points as $\overline{\phi}$, which approximates a local average in a volume enclosing the cluster of the N points. The coarse grained gradient of ϕ defined as $\overline{\phi_{,i}}$ is estimated from N points with an aid of the volumetric tensor.

With a linear approximation between two points α and β, $\overline{\phi_{,i}}$ satisfies

$$\overline{\phi_{,j}}(r_j^{(\alpha)} - r_j^{(\beta)}) = (\phi^{(\alpha)} - \phi^{(\beta)}), \tag{2}$$

where summation is taken for the repeated index j. We consider Eq. (2) for all pairs of the points. Then, the optimal value of $\overline{\phi_{,j}}$ can be determined by minimizing the following function

$$f = \frac{1}{N^2}\sum_{\alpha=1}^{N}\sum_{\beta=1}^{N}\left[\overline{\phi_{,j}}(r_j^{(\alpha)} - r_j^{(\beta)}) - (\phi^{(\alpha)} - \phi^{(\beta)})\right]^2. \tag{3}$$

The condition $\partial f/\partial\overline{\phi_{,i}} = 0$ yields

$$\frac{1}{N^2}\sum_{\alpha=1}^{N}\sum_{\beta=1}^{N}(r_i^{(\alpha)} - r_i^{(\beta)})\left[\overline{\phi_{,j}}(r_j^{(\alpha)} - r_j^{(\beta)}) - (\phi^{(\alpha)} - \phi^{(\beta)})\right] = 0. \tag{4}$$

Using $\sum_{\alpha=1}^{N}\sum_{\beta=1}^{N} r_i^{(\alpha)} r_j^{(\alpha)} = N^2 R_{ij}$ and $\sum_{\alpha=1}^{N} r_i^{(\alpha)} = 0$, we can express the coarse grained gradient $\overline{\phi_{,j}}$ with the inverse of the volumetric tensor R_{ij}^{-1} as

$$\overline{\phi_{,j}} = \frac{1}{2N^2}\sum_{\alpha=1}^{N}\sum_{\beta=1}^{N}(\phi^{(\alpha)} - \phi^{(\beta)})(r_k^{(\alpha)} - r_k^{(\beta)})R_{kj}^{-1}. \tag{5}$$

Equation (5) can be used for computing the scalar gradient when ϕ is given at $N \geq 4$ points. The reliability of Eq. (5) depends on the spatial distribution of the points. The gradient obtained by Eq. (5) is related to a low pass filtered gradient with a cutoff length $l \sim (R_a R_b R_c)^{1/3}$. The fully-resolved (unfiltered) gradient $\phi_{,j}$ is equal to $\overline{\phi_{,j}}$ when l is small enough for the cluster of the points to resolve the smallest length scale of the spatial distribution of ϕ.

2.3. Spatial gradient tensor of solenoidal vector

The gradient of vector quantity $\mathbf{u}$ is also estimated in a similar manner for all components of $\mathbf{u}$ from the following function[16]

$$f = \frac{1}{N^2}\sum_{\alpha=1}^{N}\sum_{\beta=1}^{N}\left[\overline{u_{i,j}}(r_j^{(\alpha)} - r_j^{(\beta)}) - (u_i^{(\alpha)} - u_i^{(\beta)})\right]^2, \tag{6}$$

where summation is taken for i and j. Thus, similarly to Eq. (5), we can derive the expression for the coarse grained gradient tensor $\overline{u_{i,j}} = \overline{\partial u_i/\partial x_j}$ using the volumetric tensor as

$$\overline{u_{i,j}} = \frac{1}{2N^2}\sum_{\alpha=1}^{N}\sum_{\beta=1}^{N}(u_i^{(\alpha)} - u_i^{(\beta)})(r_k^{(\alpha)} - r_k^{(\beta)})R_{kj}^{-1}. \tag{7}$$

When the vector $\mathbf{u}$ is solenoidal, the condition $\nabla \cdot \mathbf{u} = 0$ can be added as a constraint in the estimation of the gradient tensor. The optimal values of $\overline{u_{i,j}}$

under the condition $g = \overline{u_{k,k}} = 0$ are obtained using the function $F = f + 4\lambda g$ with a Lagrange multiplier λ.[16] The condition $\partial F / \partial \overline{u_{i,j}} = 0$ yields

$$\overline{u_{i,j}} = \frac{1}{2N^2} \sum_{\alpha=1}^{N} \sum_{\beta=1}^{N} (u_i^{(\alpha)} - u_i^{(\beta)})(r_k^{(\alpha)} - r_k^{(\beta)}) R_{kj}^{-1} - \lambda \delta_{ik} R_{kj}^{-1}, \tag{8}$$

where δ_{ij} is the Kronecker delta. The solenoidal condition $\overline{u_{k,k}} = 0$ is satisfied for $\overline{u_{i,j}}$ if the Lagrange multiplier is given by

$$\lambda = \frac{(1/2N^2) \sum_{\alpha=1}^{N} \sum_{\beta=1}^{N} (u_j^{(\alpha)} - u_j^{(\beta)})(r_k^{(\alpha)} - r_k^{(\beta)}) R_{kj}^{-1}}{R_{ll}^{-1}}, \tag{9}$$

where summation is taken for the repeated indices j, k, and l. The first term in Eq. (8) is identical to Eq. (7). The second term with λ corrects the gradient tensor so that the solenoidal condition is satisfied for $\overline{u_{i,j}}$.

2.4. Estimation of second derivative

We consider the estimation of second derivative from $N \geq 5$ points, where each point is identified by the integer $n(= 1, ..., N)$. From N points, we can make N different clusters each of which consists of $N - 1$ points, where the m-th cluster contains n-th points with $n \neq m$. For each cluster, we can estimate $\overline{\phi_{,j}}$ with Eq. (5). We denote the derivative estimated for the m-th cluster as $[\overline{\phi_{,j}}]^{(m)}$. The center location of the m-th cluster is given by

$$\mathbf{x}_0^{(m)} = \frac{1}{N-1} \sum_{n=1}^{N} (1 - \delta_{mn}) \mathbf{x}^{(n)}. \tag{10}$$

The spatial distribution of N clusters is characterized by the volumetric tensor R_{ij} in Eq. (1) defined with the relative location of m-th cluster $\mathbf{r}^{(m)} = \mathbf{x}_0^{(m)} - (1/N) \sum_{k=1}^{N} \mathbf{x}_0^{(k)}$. Then, by assuming that the first derivative estimated for a m-th cluster, $[\overline{\phi_{,i}}]^{(m)}$ is given at $\mathbf{x}_0^{(m)}$, we can compute the second

Table 1: DNS dataset used for testing the gradient estimation method based on the volumetric tensor. The table shows the grid size normalized by the Kolmogorov length scale $\eta = (\nu^3/\varepsilon)^{1/4}$ and turbulent Reynolds number $Re_\lambda = \sqrt{\langle u'^2 \rangle}\lambda_x/\nu$, where $\varepsilon = 2\nu\langle S_{ij}S_{ij}\rangle$ ($S_{ij} = (\partial u_i/\partial x_j + \partial u_j/\partial x_i)$: strain tensor) is the kinetic energy dissipation rate and $\lambda_x = \sqrt{\langle u'^2\rangle/\langle(\partial u'/\partial x)^2\rangle}$ is the Taylor microscale. The statistics are taken with average on a y-z plane (denoted by $\langle\ \rangle$) at $t = 130t_r$ for the mixing layers and $t = 16t_r$ for the planar jets, where t_r is the reference timescale defined as θ_M/U_M in the mixing layer and H/U_J in the planar jet. The maximum values of Re_λ are shown in the table because Re_λ changes across the mixing layer and planar jet. λ_x/η is also taken at the location of the maximum Re_λ.

	Re	$L_x \times L_y \times L_z$	$N_x \times N_y \times N_z$	$\Delta_x, \Delta_y, \Delta_z$	Re_λ	λ_x/η
Planar Jet	70000	$6H \times 10H \times 4H$	$4200 \times 5600 \times 2800$	$1.5\eta, 1.2\eta, 1.5\eta$	530	46
Mixing Layer	11000	$42\theta_M \times 54\theta_M \times 28\theta_M$	$4500 \times 5000 \times 3000$	$1.6\eta, 1.2\eta, 1.6\eta$	411	41

derivative using

$$\overline{\frac{\partial^2\phi}{\partial x_i \partial x_j}} = \frac{1}{2N^2}\sum_{\alpha=1}^{N}\sum_{\beta=1}^{N}([\overline{\phi_{,i}}]^{(\alpha)} - [\overline{\phi_{,i}}]^{(\beta)})(r_k^{(\alpha)} - r_k^{(\beta)})R_{kj}^{-1}. \tag{11}$$

A similar procedure can be used for estimating second derivatives of vectors.

3. Test of the spatial gradient estimation method based on the DNS database

3.1. Direct numerical simulations of planar jet and mixing layer

The gradient estimation method with the volumetric tensor presented in the last section are tested against the conventional finite difference approximation on Cartesian grids in turbulent flows. We use the DNS database of

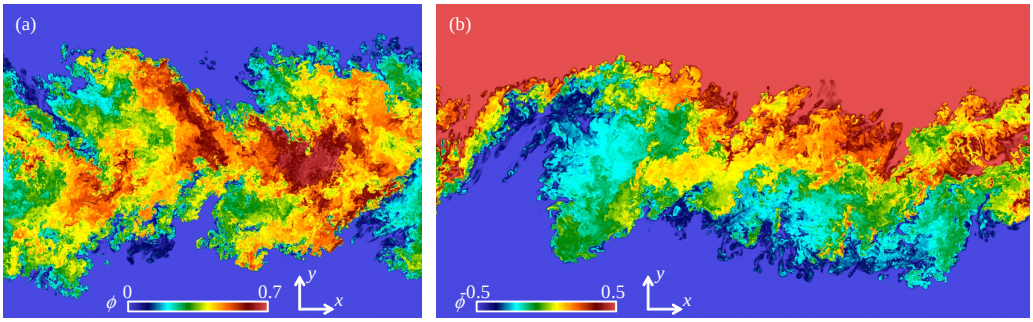

Figure 1: Passive scalar field on a x-y plane of (a) planar jet and (b) mixing layer. The gradient estimation method based on the volumetric tensor tested is on the centerline.

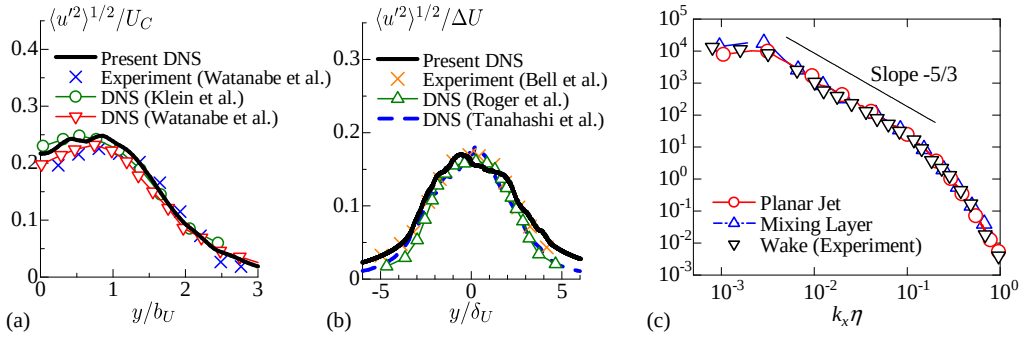

Figure 2: Self-similar profiles of rms values of streamwise velocity fluctuations $\langle u'^2\rangle^{1/2}$ in (a) planar jet and (b) mixing layer. $\langle u'^2\rangle^{1/2}$ is normalized by the mean velocity on the jet centerline U_C in (a) and the velocity difference across the mixing layer ΔU in (b). The lateral coordinate y is normalized by the jet half-width based on the mean streamwise velocity b_U or the momentum thickness δ_U of the mixing layer. Figures include the results from experiments and DNS of planar jets [18,19,20] and mixing layers. [21,22,23] (c) One-dimensional energy spectrum of streamwise velocity fluctuation, E_{uu}, on the centerline of mixing layer and planar jet. E_{uu} and wavelength k_x are normalized by ε, ν, and η. The present DNS results are compared with experiments of axisymmetric wake. [24]

incompressible temporally evolving planar jet and mixing layer with passive scalar ϕ. Detail of the present DNS can be found in our previous paper.[17] The governing equations are the Navier–Stokes equation and convective-diffusion equation of passive scalar ϕ for incompressible fluid. The flows are periodic in the streamwise (x) and spanwise (z) directions and spread with time in the cross-streamwise (y) direction, where the slip boundary conditions are applied at the lateral boundaries. The governing equations are solved by using the finite difference method for spatial discretization and a 3rd-order Runge–Kutta method for temporal advancement. The 4th-order and 2nd-order fully-conservative central difference schemes[25] are used in the periodic and cross-streamwise directions, respectively. These low order fully conservative schemes are often used in the DNS based on the finite difference method.[26,27,28] The computation domains with the size of $L_x \times L_y \times L_z$ are represented by $N_x \times N_y \times N_z$ grid points as summarized in Tab. 1. The grid spacing is uniform in the x and z directions while a finer grid spacing in the y direction is used near the center of the mixing layer and planar jet. The turbulent planar jet and mixing layer develop with time from the initial condition given by the hyperbolic tangent profile of shear layers.[17] The initial values of ϕ are $\phi = 1$ inside the jet and $\phi = 0$ outside the jet while those in the mixing layer are $\phi = 0.5$ for the upperside and $\phi = -0.5$ for the lowerside. The variables are non-dimensionalized by the initial velocity difference U_M and shear layer thickness θ_M for the mixing layer and the inlet jet velocity U_J and the jet width H for the planar jet. The Reynolds numbers Re are defined by $U_M\theta_M/\nu$ and U_JH/ν, where ν is the kinematic viscosity. The DNS are performed for the planar jet at $Re = 70,000$ and for the mixing

layer at $Re = 11,000$. The Schmidt number $Sc = \nu/D$ is 1 for ϕ (D: molecular diffusivity for ϕ). The physical and computational parameters are listed in Tab. 1, where a mean value denoted by $\langle\ \rangle$ is computed by averaging in homogeneous directions and f' denotes a fluctuation $f' = f - \langle f \rangle$. The flows are visualized with ϕ in Fig. 1, where both flows are in a self-similar state. The snapshots at this instance are used for testing the gradient estimation method with volumetric tensor. The resolutions are compared with the Kolmogorov scale on the centerline in Tab. 1, and are small enough to capture the small scale fluctuations.

A self-similar profile of the rms streamwise velocity $\langle u'^2 \rangle^{1/2}$ is compared with previous experiments and DNS in Figs. 2(a) and (b). The present DNS yields a well-known self-similar profile of the planar jet and mixing layer in agreement with previous studies. Figure 2(c) compares one-dimensional spectrum of streamwise velocity fluctuation between the present DNS and experiment of an axisymmetric wake.[24] We can find that the small scales with high wavenumbers are well resolved in the present DNS and that the normalized spectrum collapses on a single curve for all flows in an inertial subrange and dissipative scales.

3.2. Computation of spatial gradient based on the volumetric tensor from DNS data.

We estimate the gradients of passive scalar ϕ and streamwise velocity u using the volumetric tensor approximations given by Eqs. (5), (7), and (8). It should be noted that the velocity vector is solenoidal because of incompressibility. The gradients are estimated with the volumetric tensor from the DNS data by the following procedure. We consider the spherical volume

with radius R_S whose center is located on the centerline of the jet and mixing layer. The quantities computed on the grid in the DNS are interpolated onto N points which are randomly chosen in the sphere. The gradients are computed with the volumetric tensor approximation, Eqs. (5), (7), or (8), from the N points. The gradient estimated with the volumetric tensor is denoted with the subscript VT (*e.g.* $[\phi_{,j}]_{VT}$). For the same N points in the sphere, we can also calculate the coarse grained gradient directly from the interpolated value of the gradient calculated with the 4th-order finite difference approximation as $[\overline{\phi_{,j}}]_{FD} = (1/N)\sum_{n=1}^{N}\phi_{,j}^{(n)}$, where the subscript FD is used for the value computed by the finite difference. This procedure is repeated for different locations of the spheres so that we can calculate the statistics with ensemble of the spheres, where the ensemble average of the spheres is denoted by $\langle\ \rangle_R$. The estimation based on the volumetric tensor is performed for a wide range of the number of the points N ($4 \leq N \leq 300$) and the radius of the sphere R_S. We also compute the mean volume of the quasi-ellipsoid for N points defined with the volumetric tensor as $\langle V\rangle_R = \langle(4\pi/3)R_aR_bR_c\rangle_R$. A similar procedure with N points is also applied for estimating the second derivative $\overline{\partial^2\phi/\partial x^2}$ using Eq. (11).

4. Results and Discussion

4.1. Characteristics length scale of coarse grained gradient

We consider the expression for the length scale characterizing the coarse grained gradient denoted by l_C. The coarse grained gradient computed from N points with the volumetric tensor is related to the gradient averaged over N points. In the present test, the points are randomly distributed in a sphere

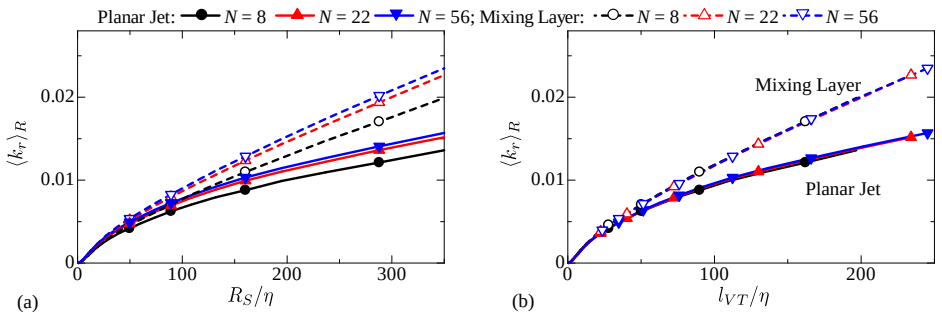

Figure 3: Averaged kinetic energy in the relative fluid motion of N points $\langle k_r \rangle_R$ plotted against (a) R_S/η and (b) l_{VT}/η.

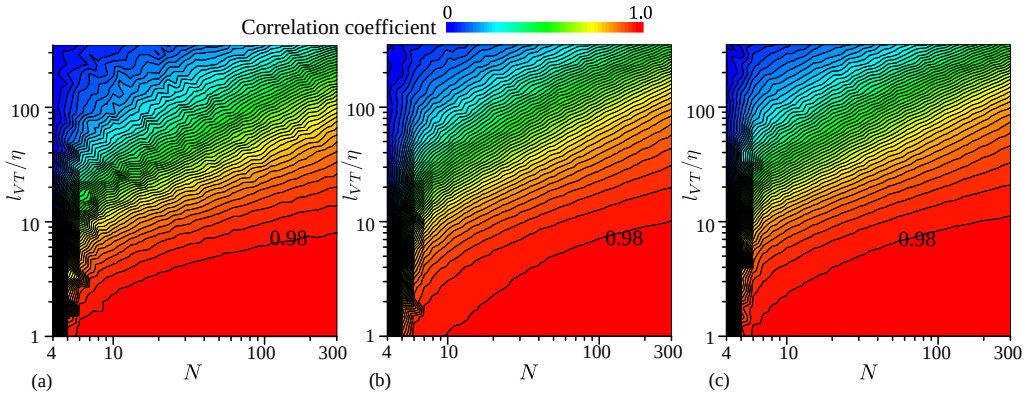

Figure 4: Correlation coefficients of coarse gradient gradients between finite difference approximation and volumetric tensor approximation in the planar jet. The correlation is plotted as a function of the number of the points, N, and the length scale of the spatial distribution of points $l_{VT} = \langle V \rangle_R^{1/3}$ determined by the volumetric tensor. (a) Scalar gradient $\overline{\phi_{,x}} = \overline{\partial\phi/\partial x}$ estimated by Eq. (5), (b) Velocity derivative $\overline{u_{,x}} = \overline{\partial u/\partial x}$ estimated by Eq. (7) without imposing the solenoidal condition, (c) Velocity derivative $\overline{u_{,x}}$ estimated by Eq. (8) with imposing the solenoidal condition. Intervals between two isolines of the correlation coefficients are 0.02.

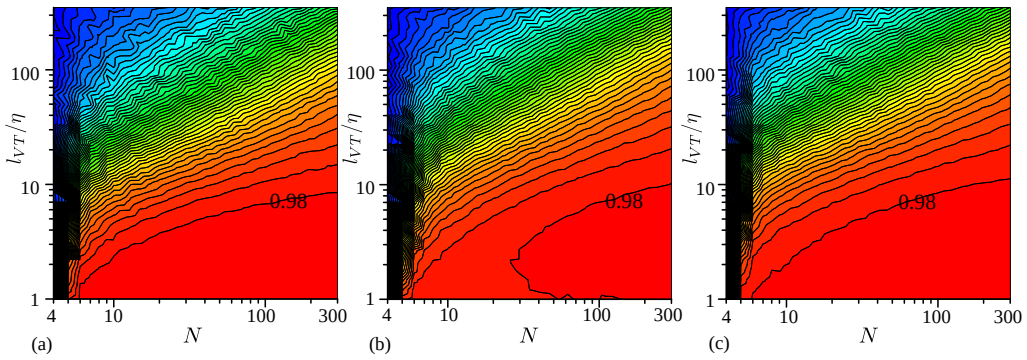

Figure 5: The same as in Fig. 4 but computed from the DNS data of the mixing layer.

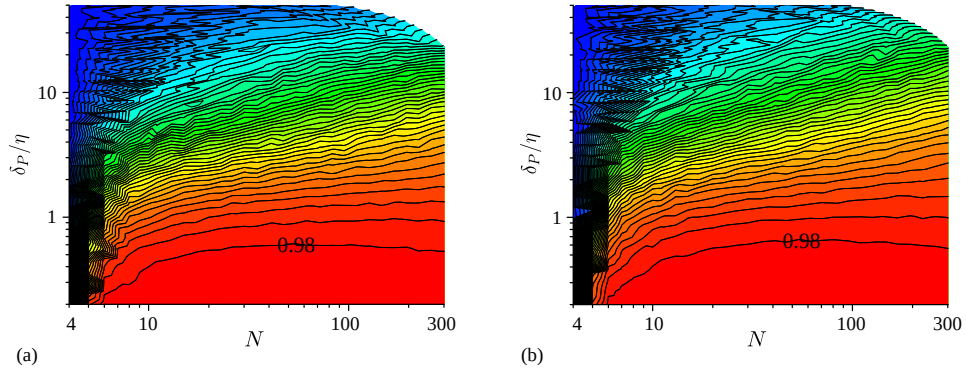

Figure 6: Correlation coefficients of coarse grained scalar gradients between finite difference approximation and volumetric tensor approximation in (a) planar jet and (b) mixing layer. The correlation is plotted against N and the characteristics distance between the points $\delta_P = (N/\langle R_a R_b R_c \rangle_R)^{-1/3}$ normalized by the Kolmogorov scale. Because δ_P decreases with N, the data is missing for large values of δ_P and N (blank in the figures).

with the radius R_S. R_S would be useful for estimating l_C if the density of the points in the sphere is large. We expect that l_C is approximated by the size of the quasi-ellipsoid defined with the eigenvalues (R_a^2, R_b^2, R_c^2) and eigenvectors of the volumetric tensor. If this is the case, the cutoff length is proportional to $V^{1/3} = [(4\pi/3)R_aR_bR_c]^{1/3}$. The relation between the average of N points and the scale can be confirmed by considering the distribution of the kinetic energy over scales in turbulence. We decompose the kinetic energy averaged over N points within the sphere into the energies in the mean motion and in the motion relative to the mean fluid motion, which are represented by $k_m = \overline{u_i}\,\overline{u_i}/2$ and $k_r = (\overline{u_iu_i} - \overline{u_i}\,\overline{u_i})/2$, respectively. The ensemble average of k_r, $\langle k_r \rangle_R$, represents the energy contained in the scale below the cutoff length of the low pass filter defined by the average of the N points.[17] $\langle k_r \rangle_R$ plotted against l_C should be independent of N for an appropriate choice for l_C. This is examined in Fig. 3, where $\langle k_r \rangle_R$ is shown as a function of R_S and $l_{VT} = \langle V \rangle_R^{1/3}$. Although $\langle k_r \rangle_R$ plotted against R_S changes with N, $\langle k_r \rangle_R$ hardly depends on N when it is plotted against l_{VT} in the jet and mixing layer. This result confirms that we can use l_{VT} as a length scale related to the coarse grained gradient obtained with the volumetric tensor.

4.2. Gradients estimated with the volumetric tensor

The correlation coefficients are calculated for the spatial gradients of ϕ and u between the volumetric tensor approximation and the finite difference approximation. We also compare the velocity gradients estimated by Eqs. (7) and (8), where the latter expression is obtained with the constraint of the solenoidal condition. The correlation coefficients for the planar jet and mixing layer are presented in Figs. 4 and 5, respectively, as a function of the

number of points N and l_{VT}/η. The correlation coefficients become large as l_{VT} decreases and N increases. The correlation coefficient for $N = 4$ is close to 0 even with small l_{VT}, and the volumetric tensor approximation with $N = 4$ points poorly estimates the gradient. The accuracy is improved significantly as N increases from 4. The coarse grained gradient becomes close to the fully resolved gradient as l_{VT} approaches the smallest length scales of u and ϕ, both of which are equal to the Kolmogorov scale η for $Sc = 1$. The correlation coefficients for $l_{VT} \approx \eta$ is almost equal to 1, indicating that the volumetric tensor approximation with small l_{VT} accurately computes the fully resolved gradient. Although two different flows are considered, the correlation coefficients plotted with l_{VT}/η are similar for the planar jet and mixing layer. This indicates that the accuracy of the gradient estimation depends on the length scale defined with the volumetric tensor. Comparison between Figs. 4(b) and (c) shows that imposing the solenoidal condition improves the estimation with the volumetric tensor for small N as attested by larger correlation coefficients for $N \approx 10$ in (c). A similar tendency can be found in the mixing layer.

The correlation coefficients are positive even for large l_{VT} and they are not small when a large number of the points are used. This is the case that the points used in the estimation are dense in the space. We consider the number of the points divided by the volume of the quasi-ellipsoid $\rho_P = N/\langle(4\pi/3)R_aR_bR_c\rangle_R$, which is related to the number density of the points. Then, the characteristics distance between the points is $\delta_P = (4\pi\rho_P/3)^{-1/3} = (N/\langle R_aR_bR_c\rangle_R)^{-1/3}$. The correlation coefficients in Figs. 4(a) and 5(a) are replotted in Fig. 6 as a function of N and δ_P/η. The dependence of the corre-

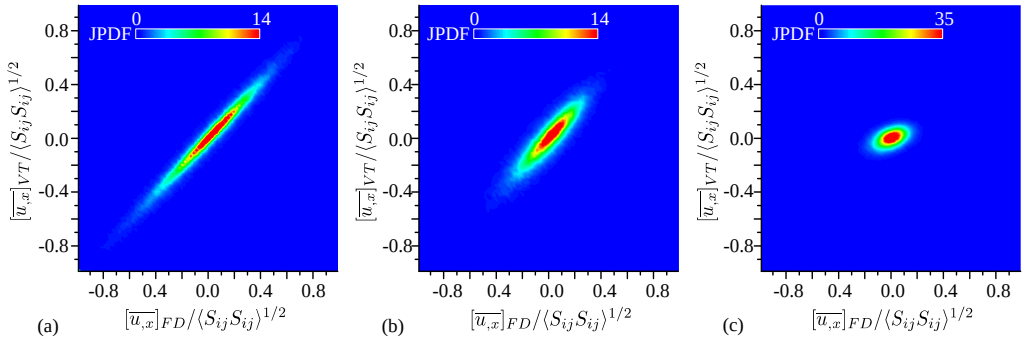

Figure 7: Joint probability density function between the finite difference value and the estimated value with the volumetric tensor with $N = 22$ points for $\overline{u_{,x}} = \overline{\partial u/\partial x}$ in the planar jet: (a) $R_S/\eta = 5$ ($l_{VT} = 3.3\eta$), (b) $R_S/\eta = 15$ ($l_{VT} = 10\eta$), and (c) $R_S/\eta = 90$ ($l_{VT} = 60\eta$). The velocity gradient is normalized by the mean strain product $\langle S_{ij}S_{ij}\rangle$.

lation on N is small for small δ_P with $N \geq 10$ in Fig. 6 while the correlation strongly depends on δ_P/η, indicating that the gradient estimation with the volumetric tensor is improved as the distance between two closest points in relation to the Kolmogorov scale is decreased. This is because velocity and scalar gradients in turbulence are mainly dominated by small scales. For example, the large scalar gradient region appears as a sheet-like structure whose thickness is closely related to η (when $Sc \approx 1$) in turbulence.[29] It should be noted that the scale of these structures can change for different Sc because the smallest scale of ϕ depends on Sc. Then, δ_P should be compared with different length scales.

The joint probability density functions (JPDFs) are calculated for $[\overline{u_{,x}}]_{FD}$ and $[\overline{u_{,x}}]_{VT}$ computed with Eq. (8). Figure 7 shows the JPDFs obtained with $N = 22$ points for $R_S = 5\eta, 15\eta$, and 90η, for which $l_{VT} = 3.3\eta, 10\eta$, and 60.0η, respectively. We can find that the estimated values by the volumetric

tensor are very close to the one computed by the finite difference for small l_{VT} even when the gradients are very large in magnitude. As l_{VT} increases (b and c) the probability for large gradients decreases because the coarse grained gradient only captures the large scale. Although the correlation becomes weaker for larger l_{VT}, $[\overline{u_{,x}}]_{VT}$ are of the same order of the ones obtained by the finite difference. This result is important in the subgrid scale modeling based on Lagrangian particles, where the coarse grained gradient is often used in the subgrid scale models. We also confirmed that the JPDFs are very similar for the scalar gradient (not shown here).

We consider the spatial distribution of the points used for the estimation of the gradient. Figure 8 shows the JPDFs of the elongation E and the planarity P for the points used for estimating the spatial gradients. When $N = 4$, P tends to be large and 4 points are located near a plane. As N increases, both P and E decrease and the spatial distribution becomes isotropic. The correlation coefficients of $\overline{\partial\phi/\partial x}$ between the volumetric tensor approximation and the finite difference approximation are calculated conditioned on the spatial distribution of the points characterized by P and E. Figure 9 compares the correlation obtained for a nearly isotropic distribution $\sqrt{E^2+P^2} < 0.4$ and anisotropic distribution $\sqrt{E^2+P^2} \geq 0.4$ in the case of $N = 4$. A positive correlation can be seen for the points with $\sqrt{E^2+P^2} < 0.4$ while the correlation coefficient is 0 for $\sqrt{E^2+P^2} \geq 0.4$. This result with the JPDF of E and P indicates that a poor gradient estimation for $N = 4$ in Figs. 4 and 5 is caused by anisotropic distributions of 4 points. The volumetric tensor approximation well estimates the gradient when the distribution of the points is nearly isotropic.

We consider the computation time of the derivative at N_P random points. The conventional approach for estimating the gradient in Lagrangian simulations is based on a finite difference on a structured grid used in an Eulerian simulation and an interpolation onto the random points.[9,30] On the other hand, the present approach allows us to directly compute the gradient from Lagrangian fluid particles which is randomly distributed in space. The computation time for the former method, T_{FD}, depends on the number of the grid points $(N_x \times N_y \times N_z)$ and the number of the random points N_P. The computation time for the volumetric tensor approximation, T_{VT}, changes depending on N_P and the number of the points used in the gradient approximation N introduced in Sec. 2. Figure 10 shows T_{VT}/T_{FD} obtained for the scalar gradient estimation for a wide range of N with $(N_x \times N_y \times N_z) = (60, 140, 40)$ and $(120, 180, 80)$ and $N_P = 6000, 10000$, and 16000. It should be noted that $(N_x \times N_y \times N_z)$ and N_P are close to the parameters used in the Lagrangian simulations of passive scalar mixing in a planar jet.[31] T_{VT}/T_{FD} tends to be large with an increase of the numbers of the points used for estimating the gradient N and of the points at which the gradient is computed N_P. An increase in the grid points also results in decrease of T_{VT}/T_{FD} because T_{FD} increases with $(N_x \times N_y \times N_z)$. Figure 6 has shown that the gradient is well estimated by the volumetric tensor approximation for $N \geq 10$. T_{VT}/T_{FD} for $N = 10$ is much smaller than 1 in most cases, or is $O(1)$ at the worst, and the volumetric tensor approximation has an advantage in a computation time. Even at $N = 30$, $T_{VT}/T_{FD} = O(10^0)$ under various conditions. T_{VT}/T_{FD} tends to increase with $\sim N^{1.8}$ for $N \geq 15$ and the volumetric tensor approximation becomes computationally too expensive for very large N.

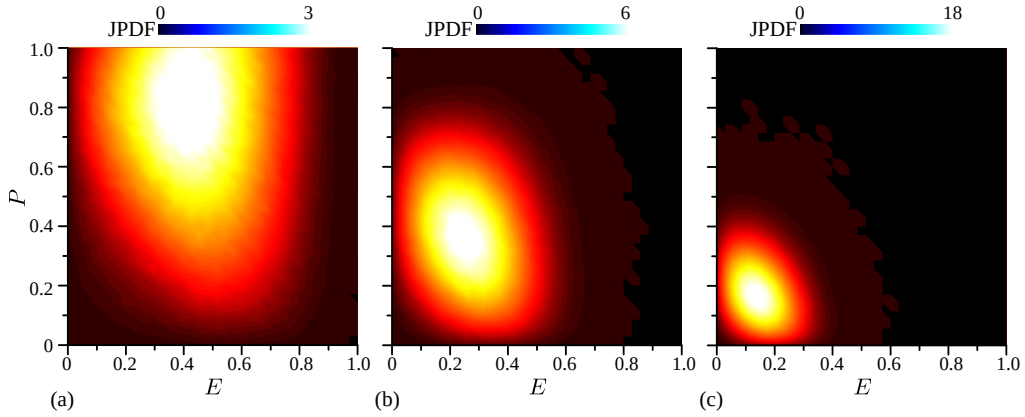

Figure 8: Joint probability density function of elongation E and planarity P of the spatial distribution of points used for estimating gradients: (a) $N = 4$, (b) $N = 8$, and (c) $N = 22$.

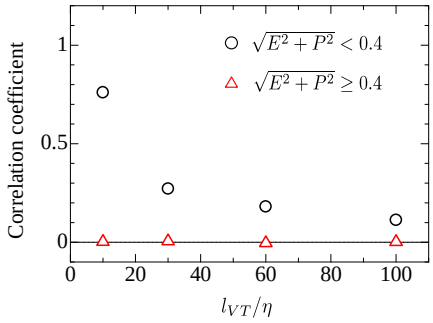

Figure 9: Dependence of volumetric tensor approximation with $N = 4$ on spatial distribution of points. Correlation coefficients of coarse grained scalar gradient between finite difference approximation and volumetric tensor approximation with $N = 4$ in the planar jet are calculated for $\sqrt{E^2 + P^2} < 0.4$ and $\sqrt{E^2 + P^2} \geq 0.4$.

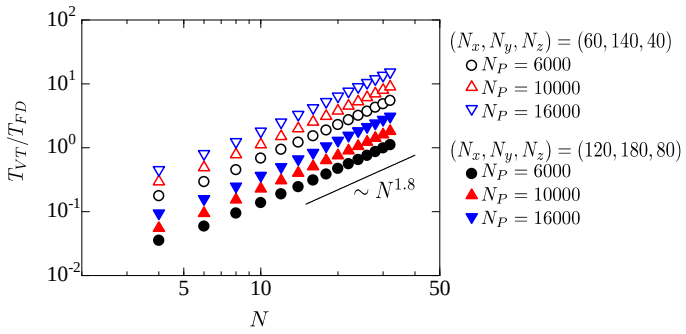

Figure 10: Ratio of computation times between volumetric tensor approximation and finite difference. Computation time for estimating scalar gradient at N_P random points is denoted by T_{VT} for the approach based on the volumetric tensor and by T_{FD} for the finite difference approach with $N_x \times N_y \times N_z$ grid points. We consider $(N_x \times N_y \times N_z) = (60, 140, 40)$ and $(120, 180, 80)$ and $N_P = 6000, 10000,$ and 16000. A solid line shows $T_{VT}/T_{FD} \sim N^{1.8}$, which is obtained with a least square method for $N \geq 15$.

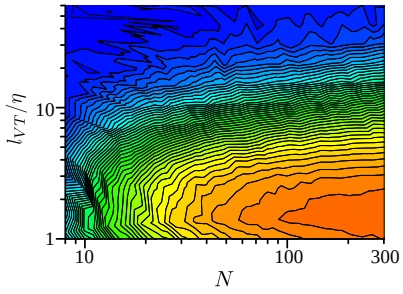

Figure 11: Correlation coefficients of second derivative $\overline{\partial^2\phi/\partial x^2}$ between finite difference approximation and volumetric tensor approximation in the planar jet. The color contour is the same as in Fig. 4.

4.3. Second derivative estimated with the volumetric tensor

With a similar method used for gradients, we calculate the correlation coefficient for $\overline{\partial^2\phi/\partial x^2}$ between the volumetric tensor approximation, Eq. (11), and the finite difference approximation. Figure 11 shows the correlation obtained from the planar jet. A positive correlation can be found in the figure, especially for large N. However, the correlation for the second derivative is weaker than that for the first derivative. Thus, the accuracy of the approximation by Eq. (11) is not as good as for the first derivative, and the second derivative should be carefully treated in the volumetric tensor approximation.

4.4. Turbulence dynamics obtained with the volumetric tensor

The velocity gradient tensor $u_{i,j} = \partial u_i/\partial x_j$ is closely related to the dynamics of turbulence.[32,33] $u_{i,j}$ has two non-zero invariants in an incompressible flow: $Q = (\omega_i\omega_i - 2S_{ij}S_{ij})/4$ and $R = -(S_{ij}S_{jk}S_{ki}/3 + \omega_i S_{ij}\omega_j/4)$. These invariants characterize the local topology.[34] The JPDF of Q and R exhibits an universal teardrop shape in various turbulent flows.[1,35,36] These invariants can be calculated with the coarse grained velocity gradient estimated with the volumetric tensor approximation as $Q_{VT} = (\overline{\omega}_i\overline{\omega}_i - 2\overline{S}_{ij}\overline{S}_{ij})/4$ and $R_{VT} = -(\overline{S}_{ij}\overline{S}_{jk}\overline{S}_{ki}/3 + \overline{\omega}_i\overline{S}_{ij}\overline{\omega}_j/4)$ with $\overline{\omega}_i = \varepsilon_{ijk}\overline{u_{k,j}}$ and $\overline{S}_{ij} = (\overline{u_{i,j}} + \overline{u_{j,i}})/2$, where ε_{ijk} is the Levi-Civita symbol. Figure 12 compares the JPDFs of Q_{VT} and R_{VT} obtained from the velocity gradients estimated with $N = 4$ and 22 at $R_S/\eta = 30$ and 100. For $Q_{VT} < 0$, the JPDF estimated with $N = 4$ tends to be large under the discriminant function $D = (27/4)R_{VT}^2 + Q_{VT}^3 < 0$ unlike the DNS results,[37,38] where the JPDF has large values on $D = 0$ with $R_{VT} > 0$. A large probability on $D = 0$ with $R_{VT} > 0$ can be seen for the JPDF estimated with $N = 22$. A local flow topology is well captured with the

velocity gradient tensor estimated with the volumetric tensor approximation when the number of points is large.

Figure 13 shows the dependence of the amplification of enstrophy and strain on the local flow topology, where the enstrophy and strain production density on a Q-R map is computed with the JPDF of Q_{VT} and R_{VT}, $P(R_{VT}, Q_{VT})$ and the average of $[\overline{\omega}_i \overline{S}_{ij} \overline{\omega}_j]_{VT}$ and $[-\overline{S}_{ij} \overline{S}_{jk} \overline{S}_{ki}]_{VT}$ conditioned on Q_{VT} and R_{VT}. It is found that a large part of enstrophy amplification occurs in a flow region with $R_{VT} < 0$ and $D > 0$ or with $R_{VT} > 0$ and $D < 0$. The enstrophy is decreased in the region with $R_{VT} > 0$ and $D > 0$. A similar result was obtained in a planar jet[39,40] and in homogeneous isotropic turbulence,[11] and the velocity gradient tensor estimated with the volumetric tensor well reproduces the dependence of the enstrophy production on Q_{VT} and R_{VT}. The local amplification of strain field occurs near the line of $D = 0$ with $R_{VT} > 0$, which also agrees with the DNS results.[11]

The kinetic energy of a relative motion of fluids $k_r = (\overline{u_i u_i} - \overline{u_i}\,\overline{u_i})/2$ is related to the kinetic energy contained in a small scale. The governing equation for k_r contains the non-linear energy transfer term $\Pi = -(\overline{u_i u_j} - \overline{u_i}\,\overline{u_j})\overline{u_{i,j}}$, which is the energy flux across scales. Figure 14 shows the average of Π_{VT} conditioned on Q_{VT} and R_{VT} computed with $N = 22$ points for various values of R_S. $\langle \Pi_{VT} | R_{VT}, Q_{VT} \rangle_R$ is positive for most values of (R_{VT}, Q_{VT}), and thus the kinetic energy is transferred from large to small scales. $\langle \Pi_{VT} | R_{VT}, Q_{VT} \rangle_R$ becomes small for very small scales in Fig. 14(a) because the viscous dissipation affects the kinetic energy at small scales. An inverse kinetic energy flux, *i.e.*, kinetic energy transfer from small to large scales, occurs for $Q_{VT} > 0$ and $R_{VT} > 0$ as attested by negative values of $\langle \Pi_{VT} | R_{VT}, Q_{VT} \rangle_R$, where the

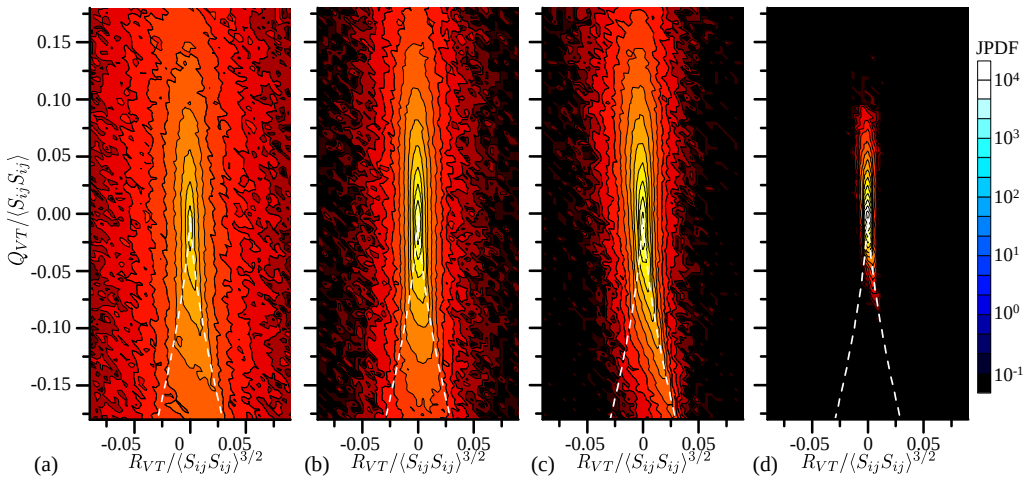

Figure 12: Joint probability density functions (JPDFs) of invariants of coarse grained velocity gradient tensor estimated with volumetric tensor approximation in the planar jet: (a) $(N, R_S) = (4, 30\eta)$ $(l_{VT} = 11\eta)$, (b) $(N, R_S) = (4, 100\eta)$ $(l_{VT} = 36\eta)$, (c) $(N, R_S) = (22, 30\eta)$ $(l_{VT} = 20\eta)$, and (d) $(N, R_S) = (22, 100\eta)$ $(l_{VT} = 67\eta)$. Broken lines denote the discriminant function $D = (27/4)R_{VT}^2 + Q_{VT}^3 = 0$. JPDFs are normalized by the mean strain product $\langle S_{ij}S_{ij}\rangle$ on the centerline.

enstrophy attenuation is dominant for the vortex stretching term. This inverse cascade was also found in homogeneous isotropic turbulence for $Q > 0$ and $R > 0$.[11] These results confirm that the volumetric approximation captures well the turbulence dynamics described by the velocity gradient tensor.

5. Conclusion

We presented the method for estimating the fully-resolved/coarse-grained gradient from randomly distributed points in turbulence. The method is based on the linear approximation of the gradients expressed with the vol-

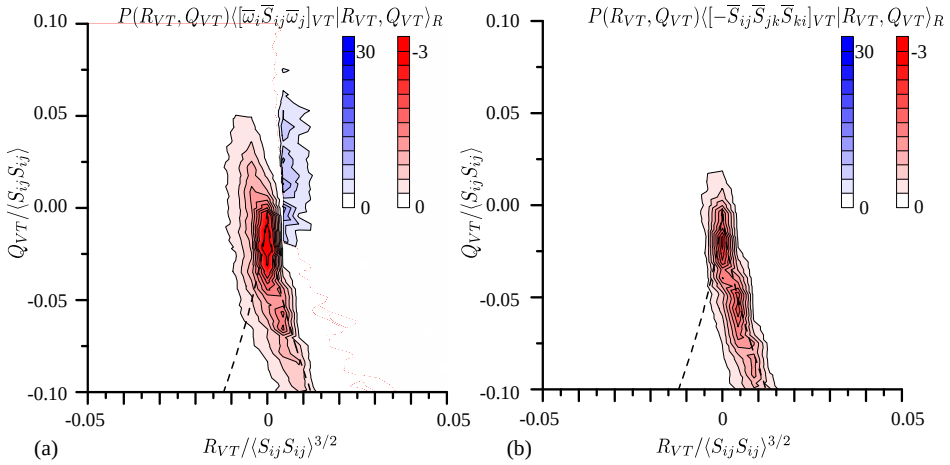

Figure 13: (a) Enstrophy production density $P(R_{VT},Q_{VT})\langle[\overline{\omega}_i\overline{S}_{ij}\overline{\omega}_j]_{VT}|R_{VT},Q_{VT}\rangle_R$ and (b) strain production density $P(R_{VT},Q_{VT})\langle[-\overline{S}_{ij}\overline{S}_{jk}\overline{S}_{ki}]_{VT}|R_{VT},Q_{VT}\rangle_R$ on a Q-R map, where $P(R_{VT},Q_{VT})$ is the joint probability function of R_{VT} and Q_{VT} and $\langle\ |R_{VT},Q_{VT}\rangle_R$ is the average conditioned on (R_{VT},Q_{VT}). The results are obtained from the velocity gradient estimated with $N=22$ and $R_S=10\eta$ ($l_{VT}=7\eta$) in planar jet. Broken lines denote the discriminant function $D=(27/4)R_{VT}^2+Q_{VT}^3=0$

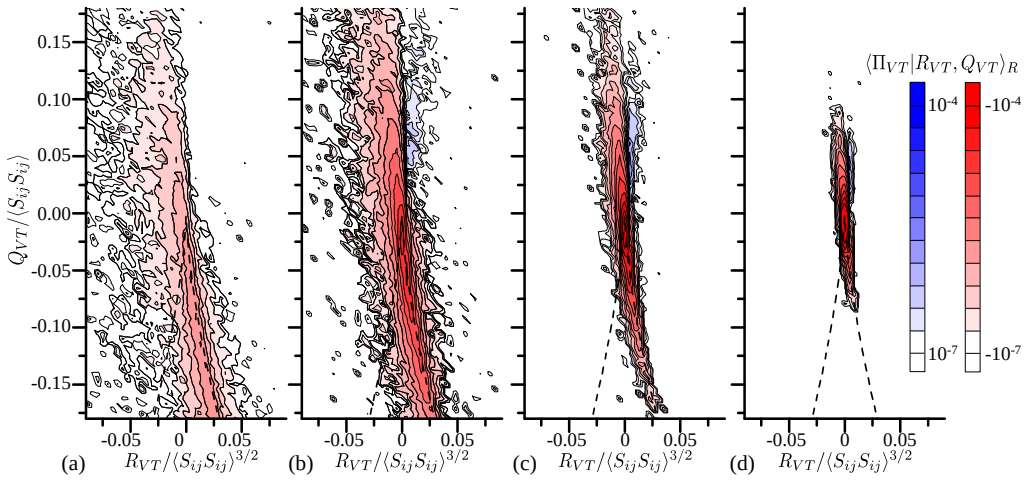

Figure 14: Kinetic energy flux across scale on a Q-R map obtained using the volumetric tensor approximation with $N = 22$: (a) $R_S = 10\eta$ ($l_{VT} = 7\eta$), (b) $R_S = 30\eta$ ($l_{VT} = 20\eta$), (c) $R_S = 60\eta$ ($l_{VT} = 40\eta$), and (d) $R_S = 100\eta$ ($l_{VT} = 67\eta$). Broken lines denote the discriminant function $D = (27/4)R_{VT}^2 + Q_{VT}^3 = 0$.

umetric tensor. The formulations were derived for the gradients of scalar, vector, and solenoidal vector and the second derivative. The coarse grained gradient is related to the low pass filtered gradient, which is obtained by averaging over multiple points. We showed that the length scale obtained by the eigenvalues of the volumetric tensor, $l_{VT} = [(4\pi/3)R_aR_bR_c]^{1/3}$, can be used as the length related to the coarse grained gradient. We tested this method based on the volumetric tensor in the turbulent planar jet and mixing layer by comparing the estimated gradients with those obtained by the conventional finite difference. It was shown that the gradients are almost the same between the volumetric tensor approximation and the finite difference approximation when the distance between the points are close compared with the smallest scale of the velocity and passive scalar fields. The volumetric tensor approximation becomes improved in terms of accuracy when more than 4 points are used in the computation because the distribution of the points tends to be isotropic for a large number of points. Although difference becomes large as the number of points decreases or as the length characterizing the point distribution l_{VT} increases, the volumetric tensor approximation still yields the gradient positively correlated to the one obtained with the finite difference. As l_{VT} increases, the magnitude of the coarse grained gradient decreases since l_{VT} is related to a cutoff length of the low pass filter. Even for large l_{VT}, the magnitude of the estimated coarse grained tensor is close between the finite difference approximation and the volumetric tensor approximation. The estimated velocity gradient well reproduces the turbulence characteristics such as local flow topology, productions of enstrophy and strain, and kinetic energy transfer across scales. The present

method is applicable to various types of Lagrangian simulations where the gradients need to be evaluated on Lagrangian particle points. In the sparse condition, under which the particle density is not high, the coarse grained gradients estimated with the volumetric tensor can be used for modeling the quantities related to the fully resolved field.[10]

Acknowledgment

The numerical simulations presented in this manuscript were carried out on the high performance computing system (NEC SX-ACE) in the Japan Agency for Marine-Earth Science and Technology. This work was partially supported by "Collaborative Research Project on Computer Science with High-Performance Computing in Nagoya University" and by MEXT KAKENHI Grant Number 16K18013.

References

[1] A. Ooi, J. Martin, J. Soria, M. S. Chong, A study of the evolution and characteristics of the invariants of the velocity-gradient tensor in isotropic turbulence, J. Fluid Mech. 381 (1999) 141–174.

[2] F. Nicoud, F. Ducros, Subgrid-scale stress modelling based on the square of the velocity gradient tensor, Flow, Turbul. Combust. 62 (3) (1999) 183–200.

[3] D. Veynante, L. Vervisch, Turbulent combustion modeling, Prog. Energy Combust. Sci. 28 (3) (2002) 193–266.

[4] P. J. Colucci, F. A. Jaberi, P. Givi, S. B. Pope, Filtered density function for large eddy simulation of turbulent reacting flows, Phys. Fluids 10 (1998) 499.

[5] M. J. Cleary, A. Y. Klimenko, J. Janicka, M. Pfitzner, A sparse-Lagrangian multiple mapping conditioning model for turbulent diffusion flames, Proc. Combust. Inst. 32 (1) (2009) 1499–1507.

[6] D. C. Haworth, Progress in probability density function methods for turbulent reacting flows, Prog. Energy Combust. Sci. 36 (2) (2010) 168–259.

[7] A. Y. Klimenko, On simulating scalar transport by mixing between Lagrangian particles, Phys. Fluids 19 (3) (2007) 031702.

[8] V. Raman, H. Pitsch, A consistent LES/filtered-density function formulation for the simulation of turbulent flames with detailed chemistry, Proc. Combust. Inst. 31 (2) (2007) 1711–1719.

[9] T. Watanabe, Y. Sakai, K. Nagata, Y. Ito, T. Hayase, LES–lagrangian particle method for turbulent reactive flows based on the approximate deconvolution model and mixing model, J. Comput. Phys. 294 (2015) 127–148.

[10] A. W. Cook, W. K. Bushe, A subgrid-scale model for the scalar dissipation rate in nonpremixed combustion, Phys. Fluids 11 (1999) 746.

[11] M. Chertkov, A. Pumir, B. I. Shraiman, Lagrangian tetrad dynamics and the phenomenology of turbulence, Phys. Fluids 11 (8) (1999) 2394–2410.

[12] G. R. Stuhne, W. R. Peltier, Vortex erosion and amalgamation in a new model of large scale flow on the sphere, J. Comput. Phys. 128 (1) (1996) 58–81.

[13] P. N. Swarztrauber, D. L. Williamson, J. B. Drake, The cartesian method for solving partial differential equations in spherical geometry, Dyn. Atmos. Oceans 27 (1998) 679–706.

[14] G. R. Stuhne, W. R. Peltier, New icosahedral grid-point discretizations of the shallow water equations on the sphere, J. Comput. Phys. 148 (1) (1999) 23–58.

[15] P. Robert, A. Roux, C. C. Harvey, M. W. Dunlop, P. W. Daly, K. H. Glassmeier, Tetrahedron geometric factors, Analysis Methods for Multi-Spacecraft Data (1998) 323–348.

[16] C. C. Harvey, Spatial gradients and the volumetric tensor, Analysis Methods for Multi-Spacecraft Data (1998) 307–322.

[17] T. Watanabe, C. B. da Silva, K. Nagata, Multi-particle dispersion during entrainment in turbulent free-shear flows, J. Fluid Mech. 805 (2016) R1.

[18] M. Klein, A. Sadiki, J. Janicka, Investigation of the influence of the Reynolds number on a plane jet using direct numerical simulation, Int. J. Heat Fluid Flow 24 (6) (2003) 785–794.

[19] T. Watanabe, Y. Sakai, K. Nagata, O. Terashima, Experimental study on the reaction rate of a second-order chemical reaction in a planar liquid jet, AIChE J. 60 (11) (2014) 3969–3988.

[20] T. Watanabe, Y. Sakai, K. Nagata, Y. Ito, T. Hayase, Enstrophy and passive scalar transport near the turbulent/non-turbulent interface in a turbulent planar jet flow, Phys. Fluids 26 (10) (2014) 105103.

[21] J. Bell, R. Mehta, Development of a two-stream mixing layer from tripped and untripped boundary layers, AIAA J. 28 (12) (1990) 2034–2042.

[22] M. M. Rogers, R. D. Moser, Direct simulation of a self-similar turbulent mixing layer, Phys. Fluids 6 (2) (1994) 903–923.

[23] M. Tanahashi, S. Iwase, T. Miyauchi, Appearance and alignment with strain rate of coherent fine scale eddies in turbulent mixing layer, J. Turbulence 2 (6) (2001) 1–18.

[24] M. S. Uberoi, P. Freymuth, Turbulent energy balance and spectra of the axisymmetric wake, Phys. Fluids 13 (9) (1970) 2205–2210.

[25] Y. Morinishi, T. S. Lund, O. V. Vasilyev, P. Moin, Fully conservative higher order finite difference schemes for incompressible flow, J. Comput. Phys. 143 (1) (1998) 90–124.

[26] R. Onishi, Y. Baba, K. Takahashi, Large-scale forcing with less communication in finite-difference simulations of stationary isotropic turbulence, J. Comput. Phys. 230 (10) (2011) 4088–4099.

[27] U. Piomelli, J. Yuan, Numerical simulations of spatially developing, accelerating boundary layers, Phys. Fluids 25 (10) (2013) 101304.

[28] J. Craske, M. van Reeuwijk, Energy dispersion in turbulent jets. Part 1. Direct simulation of steady and unsteady jets, J. Fluid Mech. 763 (2015) 500–537.

[29] K. A. Buch, W. J. A. Dahm, Experimental study of the fine-scale structure of conserved scalar mixing in turbulent shear flows. Part 2. Sc $\approx$ 1, J. Fluid Mech. 364 (1998) 1–29.

[30] . Watanabe, K. Nagata, LES–Lagrangian-particles-simulation of turbulent reactive flows at high Sc number using approximate deconvolution model, AIChE J. 62 (8) (2016) 2912–2922.

[31] T. Watanabe, K. Nagata, Mixing model with multi-particle interactions for Lagrangian simulations of turbulent mixing, Phys. Fluids 28 (8) (2016) 085103.

[32] A. Tsinober, An informal conceptual introduction to turbulence, Springer, 2009.

[33] C. Meneveau, Lagrangian dynamics and models of the velocity gradient tensor in turbulent flows, Annu. Rev. Fluid Mech. 43 (2011) 219–245.

[34] M. S. Chong, A. E. Perry, B. J. Cantwell, A general classification of three-dimensional flow fields, Phys. Fluids 2 (5) (1990) 765–777.

[35] J. Soria, R. Sondergaard, B. J. Cantwell, M. S. Chong, A. E. Perry, A study of the fine-scale motions of incompressible time-developing mixing layers, Phys. Fluids 6 (2) (1994) 871–884.

[36] C. B. da Silva, J. C. F. Pereira, Invariants of the velocity-gradient, rate-of-strain, and rate-of-rotation tensors across the turbulent/nonturbulent interface in jets, Phys. Fluids 20 (5) (2008) 055101.

[37] A. Naso, A. Pumir, Scale dependence of the coarse-grained velocity derivative tensor structure in turbulence, Phys. Rev. E 72 (5) (2005) 056318.

[38] O. R. H. Buxton, S. Laizet, B. Ganapathisubramani, The interaction between strain-rate and rotation in shear flow turbulence from inertial range to dissipative length scales, Phys. Fluids 23 (6) (2011) 061704.

[39] O. R. H. Buxton, B. Ganapathisubramani, Amplification of enstrophy in the far field of an axisymmetric turbulent jet, J. Fluid Mech. 651 (2010) 483–502.

[40] R. R. Taveira, J. S. Diogo, D. C. Lopes, C. B. da Silva, Lagrangian statistics across the turbulent-nonturbulent interface in a turbulent plane jet, Phys. Rev. E 88 (4) (2013) 043001.